Solar-Terrestrial Physics. 2022. Vol. 8. Iss. 2. P. 3–9. DOI: 10.12737/stp-82202201. © 2022
A.T. Altyntsev, N.S. Meshalkina, I.I. Myshyakov. Published by INFRA-M Academic Publishing House

UDC 523.9-7, 523.98
DOI: 10.12737/stp-82202201

Received March 23, 2022
Accepted May 4, 2022

COHERENT MICROWAVE EMISSION AS AN INDICATOR OF NON-THERMAL ENERGY RELEASE AT A CORONAL X-RAY POINT

A.T. Altyntsev
Institute of Solar-Terrestrial Physics SB RAS, Irkutsk, Russia, altyntsev@iszf.irk.ru

I.I. Myshyakov
Institute of Solar-Terrestrial Physics SB RAS, Irkutsk, Russia, ivan_m@iszf.irk.ru

N.S. Meshalkina
Institute of Solar-Terrestrial Physics SB RAS, Irkutsk, Russia, nata@iszf.irk.ru

Abstract. A response has been found in a narrow band 5–7 GHz of microwave emission to the appearance of a coronal X-ray point. The emission source is a short X-ray loop located in the tail part of an active region and occurring when magnetic fields are reconnected near the footpoints of high and low loops rooted in nearby magnetic pores of the opposite polarity. The power of energy release is low and no response of the hot plasma component was observed in hard X-rays. Analysis of images in soft X-ray and extreme UV radiation shows that microwave emission has a coherent nature and is generated at a frequency of about twice the plasma frequency by electrons with energies above several tens of keV. The result indicates a high diagnostic potential of microwave observations to detect acceleration processes in weak transitory events and can be useful for observation planning with new generation radioheliographs currently under development.

Keywords: Sun, coronal points, microwave bursts, coherent emission, jets.

INTRODUCTION

Strong magnetic fields are concentrated in solar active regions. These dynamic complex magnetic structures emerge in the photosphere and extend to the corona, which is a source of extreme solar events such as solar flares and coronal mass ejections. Along with powerful flares, weak disturbances of various spatial and temporal scales are generated in the corona and transition region. These disturbances show up as weak brightenings in soft X-ray [Lin et al., 1984; Shimizu et al., 1994] and in the extreme ultraviolet (EUV) ranges [Porter et al., 1984; Young et al., 2018]. Observations of hard X-ray bursts have revealed that the non-thermal electron component is generated in microflares [Schadee et al., 1983; Christe et al., 2008; Hannah et al., 2008, 2011; Wright et al., 2017]. Interest in studying low-power events has been stimulated by the fact that their combination can make a major contribution to the heating of the corona.

Dissipation of magnetic tension and dissipation of MHD waves are discussed as the main mechanisms of corona heating (see, e.g., reviews [Aschwanden, 2004; Mandrini et al., 2000; Klimchuk, 2006]). The occurrence of non-thermal emission is naturally associated with the dissipation of magnetic tension, among the mechanisms of which two groups are distinguished. In the first group, energy release is provided by the dissipation of currents in layers formed in the corona due to interactions between thin elementary loops or threads [Parker, 1988; Lopez Fuentes, Klimchuk, 2010]; in the second group, relaxation occurs through Joule heating of currents induced by magnetic fields of moving loop footpoints [Gudiksen, Nordlund, 2005; Warnecke, Peter, 2019].

Together with EUV and hard X-ray data, observations in the radio frequency band can provide unique information on corona heating. First, radio emission parameters depend on the magnetic field in the source; second, radio observations are more sensitive to the appearance of non-thermal electrons [Benz, 1986; Gopalswamy et al., 1997; Fleishman, Melnikov, 1998; Altyntsev et al., 2012]. It has long been noticed that in active regions along with gyroresonance emission of thermal plasma over sunspots with strong magnetic fields there is microwave emission generated by other mechanisms. The first signs of non-thermal emission were observed by the Westerbork Synthesis Radio Telescope at a frequency of 5 GHz during the formation of sunspots in active regions [Shibasaki et al., 1983; Chiuderi Drago et al., 1987]. At a frequency of 5.7 GHz, a response to the occurrence of sunspots was observed with the Siberian Solar Radio Telescope (SSRT). It has been found that in many cases the smooth increase in radio emission is superimposed by ~20 min bursts with an amplitude less than 1 s.f.u. [Nefed'ev et al., 1993; Myachin et al., 1999]. The free-free emission as a burst emission mechanism was first proposed by White et al. [1995] on the basis of temperature and emission measure estimates from soft X-ray emission.

VLA observations at frequencies of 8.3 and 15 GHz have confirmed that in addition to thermal gyroresonance and free-free emission there are non-thermal

emission bursts synchronous with X-ray microflares [Gopalswamy et al., 1997]. Durations of weak microwave bursts (short-term microwave brightenings or bright coronal points) were 1–10 min, and amplitudes of the fluxes were sometimes lower than 0.025 s.f.u. The authors proposed a scenario in which the bursts were caused by heating or particle acceleration in compact magnetic loops. Observations of weak microwave bursts in a wide spectral range have been made at the Radio Observatory OVSA [Gary et al., 1997; Nindos et al., 1999]. Observations of several tens of microflares recorded by the Nobeyama Radioheliograph (NoRH) have been discussed in [Kundu et al., 2006]. Altyntsev et al. [2020] have explored weak energy release processes in the corona over an isolated active region. They manifested themselves as a quasi-stationary increase in microwave and soft X-ray emissions, accompanied by a series of class B and C microflares. Multiwave microwave observations have distinguished a pulse nonthermal component at frequencies below 6 GHz against the background of thermal free-free emission of microflares.

In this paper, we discuss the unusually narrow-band microwave emission of a bright coronal X-ray point associated with a coronal plasma jet observed in AR 12738 on April 13, 2019.

INSTRUMENTS AND METHODS

Microwave emission sources have been localized using a 48-antenna prototype of the Siberian Radioheliograph (SRH-48) at five frequencies (4.5, 5.2, 6.0, 6.8, and 7.5 GHz) with a time cadence of 8.4 s [Lesovoi et al., 2014, Lesovoi et al., 2017]. The SRH beam width was down to 100″ and varied inversely with frequency. To measure the spectrum, we have used data from the Badary Broadband Microwave Spectropolarimeter (BBMS) located in Badary [Zhdanov, Zandanov, 2011] with a frequency band 4–8 GHz. Sequences of NoRH images obtained at a frequency of 17 GHz [Nakajima et al., 1994] were employed to study the spatial distribution and variations of emission intensity. The spatial resolution was down to 10″.

Soft X-ray sources were localized using data from the X-ray Telescope (XRT) aboard the Hinode satellite [Kosugi et al., 2007]. XRT is sensitive in the energy range from ~0.15 to more than 3 keV and can detect plasma emission with a temperature from ~1 MK to several tens of MK. The data on spectral and spatial characteristics of EUV emission was recorded by the Solar Dynamic Observatory (SDO) [Pesnell et al., 2012]. We used full solar disk images with a resolution of 0.6″ recorded every 12 s (AIA) [Lemen et al., 2012]. Six EUV channels of SDO/AIA (171, 193, 211, 131, 335, and 94 Å) have been used to calculate emission measures at temperatures $5.5<\lg T<7.5$. The differential emission measure was calculated by the inversion method [Cheng et al., 2012].

The coronal magnetic field was calculated with the aid of the potential field approximation based on Green's function. Input boundary conditions were taken from SDO/HMI vector magnetograms (series B 720s) [Scherrer et al., 2012; Schou et al., 2012]. π-ambiguity was eliminated by the method proposed in [Rudenko, Anfinogentov, 2014]. The potential field was extrapolated in spherical geometry for a uniform grid with a resolution of 1 Mm.

ANALYSIS OF OBSERVATIONS

The dynamic spectrum of microwave emission recorded by BBMS between 05:43:30 and 06:15:00 UT (hereinafter Universal Time is also used) is shown in Figure 1. The ~2 GHz band of enhanced emission is seen around a frequency of 6 GHz, at which the maximum flux is 8 s.f.u. The enhancement interval lasts for about 15 min. At the beginning of this interval there is a slight increase in the flux in the GOES soft X-ray channel. In the GOES hard X-ray channel and the Fermi Gamma-ray Burst Monitor signals [Meegan et al., 2009] there is no flux increase.

During the time interval of interest there is one active region AR 12738 on the solar disk. The magnetic structure of the active region consists of a large leading sunspot of S polarity and a mixture of small magnetic sunspots of different signs distributed along the tail (Figure 2, *a*). During brightening of the microwave emission in Figure 1, *a*, a bright sunspot appears in the

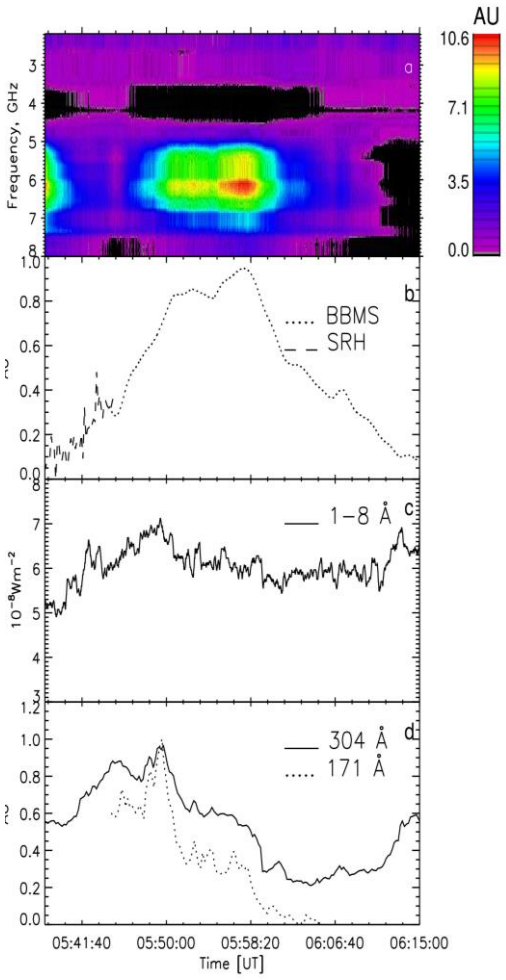

Figure 1. Dynamic spectrum in the microwave range recorded by BBMS on April 13, 2019 (*a*); a normalized flux at 6 GHz according to BBMS data and an SRH correlation plot to 05:45:15 (*b*); GOES data smoothed with a window of 10 s (*c*); EUV fluxes at 304 and 171 Å (SDO/AIA) calculated from the region marked with the dotted frame in Figure 2, *a* (*d*)

XRT/Hinode soft X-ray image, which is a short bright loop A marked with an arrow in Figure 2. Later, as shown in the upper right corner of Figure 2, *a*, the bright sunspot in this place disappears. The distance between footpoints of loop A is ~20″ with its width up to 4″. The dotted frame marks borders of the images *b*, *c*. The time dependence of the 304 Å flux summed over this frame (see Figure 1, *c*) shows a simultaneous increase in the intensity of the EUV and soft X-ray emission.

The SRH observations were available until 05:45:15. Microwave sources at a frequency close to 6 GHz are marked with white contours in Figure 2, *b*. The contours indicate the sources in the last image, recorded by SRH-48 at a frequency of 5.1 GHz at 05:44:51 at the beginning of an increase in the microwave emission. The contours enclose the leading southern spot and bright structures in the image at a wavelength of 193 Å, including loop A. The SRH-48 beam pattern (oval in the lower left corner of Figure 2, *b*) is too large for accurate localization of a weak microwave source. A higher spatial resolution is provided by observations in the EUV and microwave ranges at the frequency of 17 GHz (Figure 2, *c*). Source A is faint in the brightness temperature distribution at 17 GHz (blue contours), but it is the brightest on the difference map (yellow contours). In source A, the brightness temperature increases from $14 \cdot 10^3$ to $18.5 \cdot 10^3$ K. A similar pattern with the maximum brightness in loop A is observed on the difference maps of the emission measure calculated from EUV images.

The difference map in the 193 Å line is shown in Figure 3, *a*. Near region A are seen to be northeastern footpoints of short bright loops, which are observed at different SDO/AIA wavelengths. Analysis of the maps has revealed that these loops produce ejections several times, modulating brightness of the EUV emission. Corresponding peaks are seen on the 304 Å light curve in Figure 1, *d*, which represents the profile of the EUV flux from the area marked with the dotted frame in Figure 2, *a* and the black solid frame in Figure 3, *a*. The ejection is shown in more detail in Figure 3, *b*, where an eruptive loop with a twist at the top can be seen.

We can estimate the plasma parameters at the energy release site, using a differential emission measure (DEM). The DEM curves calculated in the minimum and maximum 304 Å flux for the area bounded by the frame in Figure 2, *b* are presented in Figure 4, *a*. The plasma temperature T=1.5−2 MK, and in both cases there is no hot component above 8 MK. With the emission measure $EM=2 \cdot 10^{28}$ cm^{-5}, the plasma density should be $\sim 5 \cdot 10^{10}$ cm^{-3}.

Knowing the temperature and the emission measure makes it possible to calculate the brightness temperature $T_{\rm br}$ of the thermal free-free emission [Zhang et al., 2001]:

$$T_{\rm br} = 0.2 f^{-2} T^{-0.5} EM + T_{\rm q},$$

where $T_{\rm q}$ is the temperature of the quiet solar disk at a frequency f. At 17 GHz, $T_{\rm br} \approx 20 \times 10^4$ K for $T_{\rm q}=10^4$ K, which is close to the observed value.

The appearance of the non-thermal electron component follows from observations of the microwave spectrum recorded with the BBMS spectrometer. The spectrum for the profile maximum at 6 GHz (05:58) is shown in Figure 4, *b*. The background emission at 05:45 is subtracted here. The flux reaches ~8 s.f.u., and the noise level is ~1–2 s.f.u. The spectrum width does not exceed 2 GHz. The spectrum exhibits a steep slope toward low and high frequencies. At frequencies above 7.5 GHz, the amplitude of the spectrum increases again, yet measurements at these frequencies are unreliable.

DISCUSSION

The purpose of this work is to search for indicators of non-thermal energy release in weak transient events. We have found an interval of ~15 min in which a narrow-band microwave emission with a flux up to 8 s.f.u. at 6 GHz was observed during the existence of coronal X-ray point A.

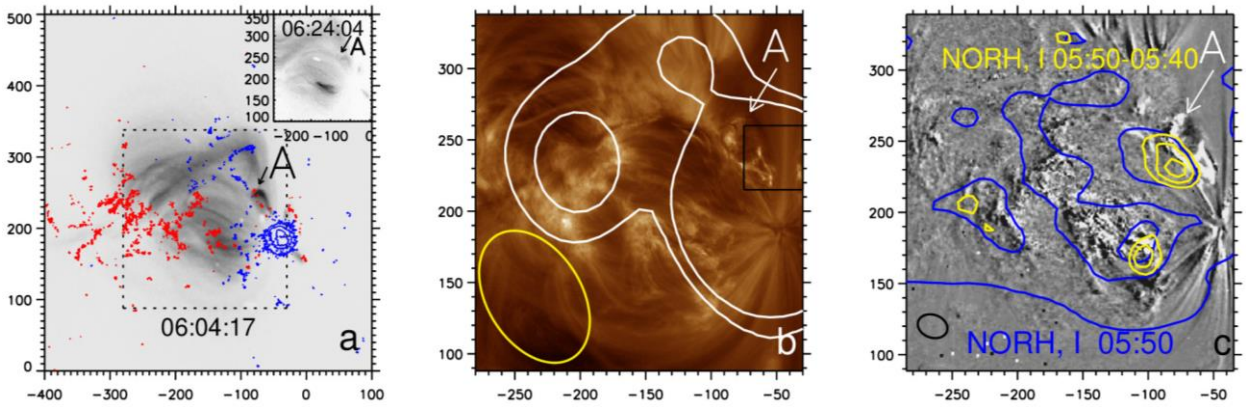

Figure 2. AR 12635 in soft X-ray emission (XRT/Hinode) at 06:04 and 06:24 (frame in the upper right corner) and magnetic field components along the line of sight ±100, ±300, ±1000, ±1500 G (*a*): red and blue contours are positive and negative components respectively; the dotted frame bounds the area shown in panel *b*. Image at 193 Å for 05:50 (*b*): white contours indicate the brightness temperature ($6.9 \cdot 10^4$, $9.4 \cdot 10^4$ K)·at 5.1 GHz for 05:44:51; the yellow oval in the lower corner is the SRH beam pattern. The difference map of the emission measure at 05:40 and 05:50 (*c*): blue contours are the distribution of the brightness temperature in the image at 17 GHz; yellow contours are the 0.5, 0.7, 0.9 levels of the maximum difference between the images at 17 GHz for 05:40 and 05:50; the black oval in the lower left corner is the NoRH beam pattern. Here and in Figures 3, 5, coordinates are given in arcseconds from the solar disk center.

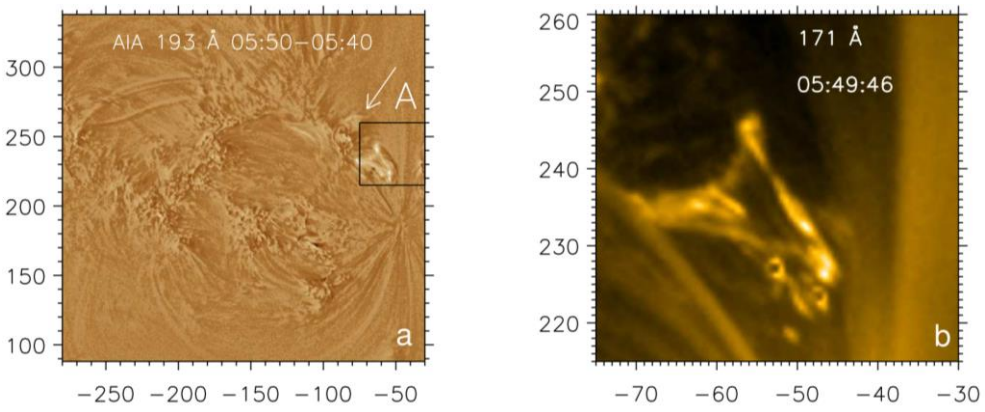

Figure 3. Difference between images at 193 Å for 05:40 and 05:50 (*a*), the black frame marks the area shown in panel *b*; the eruptive loop in the image at 171 Å (SDO/AIA) for 05:49:46 (*b*)

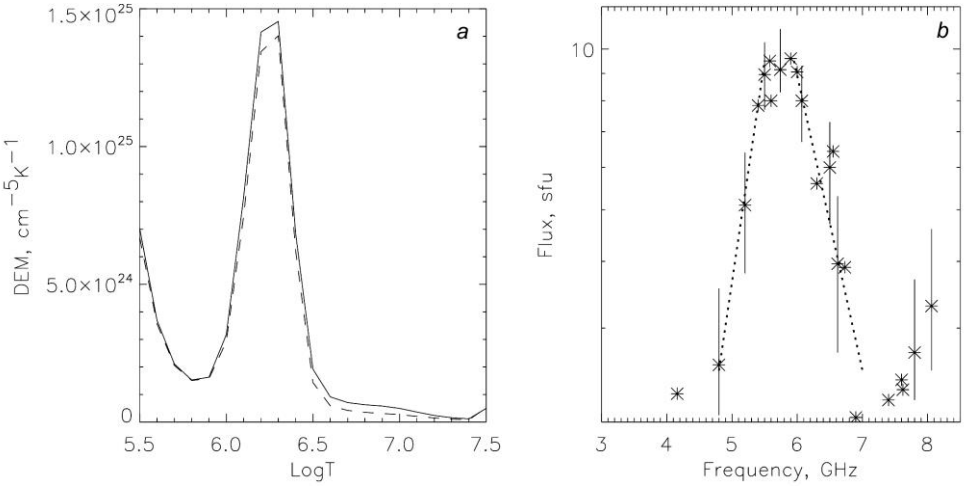

Figure 4. Differential emission measure calculated for the moments before a burst (05:40) and at a maximum (05:50) of the profile at 304 Å (*a*); difference between the microwave spectra constructed for 05:45 and 05:58 (*b*). Vertical marks show the noise level on flux curves

A feature of this region follows from calculations of the neutral line of the radial magnetic field component in four different spherical layers above the surface of the photosphere (Figure 5). The small-scale magnetic field disappears rapidly with height (panels *b*, c), and a vast region of negative magnetic fields remains, including the main sunspot, except for the compact spot of positive polarity near feature A.

The X-ray image shows that the footpoints of high loops with negative polarity and the footpoint of a low bright loop with positive polarity are closely spaced there. As follows from Figure 5, *d*, the height of the low loop does not exceed 9 Mm; at this height the positive inclusion on the vertical-field maps disappears. The estimated magnetic field in the low loop is ~100 G. A scenario of minifilament eruption and flow generation in a similar configuration due to magnetic reconnection of antiparallel fields near loop footpoints has been proposed in [Shibata et al., 1992; Yokoyama, Shibata, 1995, 1996; Panesar et al., 2017, 2018]. A short loop is formed in the region of primary reconnection, which can be identified with the low X-ray loop in Figure 5.

In the microwave emission at frequencies around 6 GHz there was no response to the eruption. It can therefore be assumed that the microwave emission was generated by accelerated electrons in the X-ray loop resulting from reconnection. On the microwave maps at 17 GHz, this region stands out for its brightness due to the enhanced free-free emission because of an increase in plasma density in the loop.

Assuming that the microwave flux of 8 s.f.u. is emitted from the 4″×20″ loop A, its brightness temperature T_{br} can be estimated as 5×10^7 K at 6 GHz. Such a high value of T_{br} indicates the non-thermal nature of microwave emission since, according to EUV measurements, the plasma temperature in the loop does not exceed 2 MK. There are also no signs of plasma heating to high temperatures in the GOES 0.5–4 Å channel, which is sensitive to the appearance of plasma with a temperature above 4 MK [Thomas et al., 1985].

In solar flares, a high brightness temperature of microwave emission is generally achieved through gyrosynchrotron emission of weakly relativistic electrons in a magnetic field. In our case, a too narrow spectral band $\Delta f/f\approx0.25$ does not correspond to this mechanism. The steepness of the fall in the observed spectrum at frequencies above maximum gives an estimate of the rate of decrease in the energy distribution of non-thermal electrons. In the case of a power-law isotropic spectrum, the slope index should exceed $\delta \approx 6.5$.

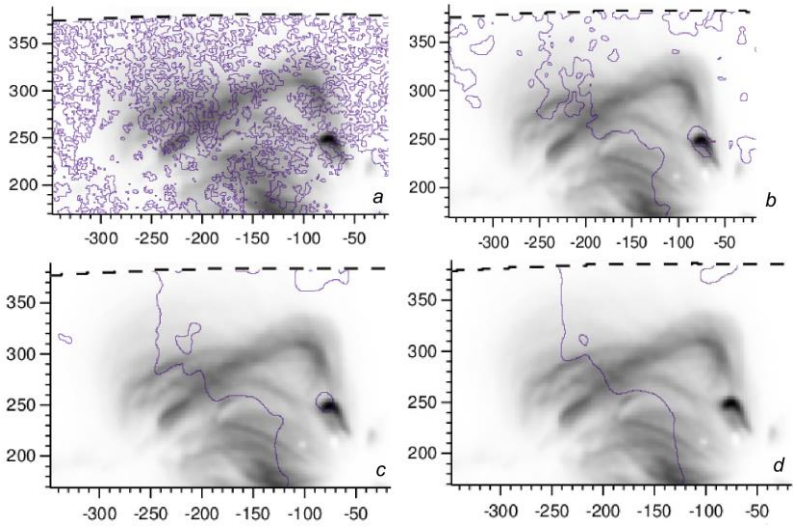

Figure 5. Reconstruction of neutral lines of a radial magnetic field (contours) in various spherical layers (*a* — 0; *b* — 3 Mm; *c* — 6 Mm; *d* — 9 Mm) above the photosphere surface. The thickened dashed line indicates the computational domain. Background is an XRT/Hinode image turned by 06:04:17

On the other hand, in our case $f_{pe}\approx 7\, f_{ce}$, where the cyclotron frequency $f_{ce}=2.8\times10^8$ Hz with a magnetic field in a loop of 100 G, and the plasma frequency $f_{pe}=2^{10.9}$ Hz at $n=5\cdot10^{10}$ cm^{-3}. In this case, the gyrosynchrotron emission is suppressed by several orders of magnitude due to the Razin effect [Ginzburg, Syrovatskii, 1965]. At the same time, in order to obtain the observed emission flux of the order of ten s.f.u. with a steep fall $\delta\approx6.5$ there have to be an abnormally large number of non-thermal emitting electrons, which contradicts the absence of responses in the GOES hard X-ray channel and in sensors of the Fermi X-ray spectrometer.

If $f_{pe}>>f_{ce}$, the narrow-band emission can be generated at the main plasma frequency or its harmonic. At frequencies above 3 GHz, the second-harmonic emission dominates, at which collisional absorption of electromagnetic waves is significantly lower [Benz et al., 1992; Zaitsev et al., 1997]. The plasma density required for the 6 GHz emission is about 10^{11} cm^{-3}, which is close to the above estimate. We should note some works in which a coherent narrow-band emission generated by non-thermal electrons at frequencies around 6 GHz was observed at a doubled plasma frequency during type III spikes [Altyntsev et al., 2007; Meshalkina et al., 2012].

Cases with stationary narrow-band emission were detected at decimetric wavelengths [Zaitsev et al., 1997; Yasnov et al., 2003] and were interpreted as a consequence of the excitation of upper hybrid waves through pitch-angular anisotropy of non-thermal electrons. The loss-cone anisotropy is established when the electron relaxation time exceeds the time of its passage through the loop. At $n\approx10^{11}$ cm^{-3}, the anisotropy manages to establish itself in the angular distribution of electrons with energies above tens of keV [Trubnikov, 1965]. If this energy is exceeded, we can also ignore the relaxation of the non-thermal electron energy. The cone instability can be excited if its increment $\gamma\approx2\pi\, f_{pe} n_{ac}/n$ (n_{ac} is the electron density with an energy >20 keV) exceeds the Coulomb collision frequency and the non-linear damping rate [Zaitsev, Stepanov, 1983]. Non-linear damping depends primarily on the background plasma temperature and is negligible at 2 MK. The Coulomb collision rate is determined by the background plasma density and temperature and is 10^3 s^{-1}. Thus, the ratio between densities of accelerated and thermal electrons should exceed $3\cdot10^{-8}$. From the expressions derived in [Zaitsev, Stepanov, 1983] it follows that in order to achieve an effective radio brightness of $\sim10^8$ K in loop A, $n_{ac}/n\geq10^{-6}$; and the energy storage of non-thermal electrons is small compared to that of the background plasma.

Note that magnetic reconnection and electron acceleration may be accompanied by the occurrence of plasma turbulence of different types in the energy release region. Scattering of non-thermal electrons by turbulent fluctuations of electric and magnetic fields should give rise to incoherent electromagnetic emission. In the case of small-scale plasma turbulence, resonant transient radiation with a sufficiently narrow band near $f_{pe}\left(1+ f_{ce}^2 / f_{pe}^2\right)$ may appear [Fleishman, 2001; Fleishman et al., 2005]. This mechanism is used to explain narrow-band UHF flare bursts. To generate emission at 6 GHz, the plasma density in the source must exceed the above estimate by an order of magnitude. Moreover, as mentioned above, the centimeter emission with a frequency close to the fundamental plasma one is rapidly absorbed due to Coulomb collisions in the vicinity of the source.

Scattering of fast electrons due to magnetohydrodynamic turbulence in the region of flare acceleration of electrons can also generate narrow-band emission [Li, Fleishman, 2009]. The typical emission frequency is higher than the plasma frequency by a factor proportional to the root of the ratio of the characteristic energy of emitting electrons to the background plasma temperature. At such frequencies, collisional absorption is small and does not prevent emission from leaving the source. The intensity of such diffusive synchrotron emission is pro-

portional to the number of fast electrons and depends radically on the level and spectrum of magnetic fluctuations. In our case, the level of magnetic fluctuations with an amplitude comparable to the magnetic field strength in the loop (~ 100 G) is required.

CONCLUSION

An unusually narrow-band radio emission in the 5–7 GHz band was detected in the dynamic spectra obtained with BBMS. We managed to establish a link between the occurrence of this emission and the brightening of a coronal X-ray point. Analysis of soft X-ray and EUV images and magnetic field calculations allow us to conclude that the coronal point is a low loop that occurs when magnetic fields of complexes of long and short loops, rooted in close spots or pores of opposite polarity, reconnect. During the reconnection, filament eruption and flow formation were observed in EUV, the response to which was not manifested in soft X-ray and microwave emissions.

Estimates show that characteristics of the spectrum of microwave emission of a bright X-ray point indicate a coherent mechanism of emission of electrons with energies above several tens of keV at the harmonic of plasma frequency. Thus, observations have a high diagnostic potential for detecting non-thermal energy release channels in transient events. It is hoped that observations with new generation SRH, MUSER, and eOVSA radioheliographs will contribute to the realization of this potential.

We are grateful to Grigory Fleishman and Hamish Reid for useful discussions. We also thank the teams of the Solar Dynamic Observatory, GOES, the Nobeyama Observatory, the ISTP SB RAS Radioastrophysical Observatory for providing the data. The work was financially supported by RSF (Grant No. 22-22-00019).

REFERENCES

Altyntsev A.T., Grechnev V.V., Meshalkina N.S., Yan Y. Microwave type III-like bursts as possible signatures of magnetic reconnection. *Solar Phys.* 2007, vol. 242, iss.1-2, pp. 111–113. DOI: 10.1007/s11207-007-0207-9.

Altyntsev A.T., Fleishman G.D., Lesovoi S.V., Meshalkina N.S. Thermal to nonthermal energy partition at the early rise phase of solar flares. *Astrophys. J.* 2012, vol. 758, p. 138. DOI: 10.1088/0004-637X/758/2/138.

Altyntsev A.T., Meshalkina N.S., Fedotova A.Ya., Myshyakov I.I. Background microwave emission and microflares in young active region 12635. *Astrophys. J.* 2020, vol. 905, iss. 2, 149. DOI: 10.3847/1538-4357/abc54f.

Aschwanden M.J. *Physics of the Solar Corona. An Introduction*. Chichester: Praxis Publishing Ltd.; Berlin: Springer-Verlag, 2004, 924 p.

Benz A.O. Millisecond radio spikes. *Solar Phys.* 1986, vol. 104, p. 99. DOI: 10.1007/BF00159950.

Benz A.O., Magun A., Stehling W., Su H. Electron beams in the low corona. *Solar Phys.* 1992, vol. 141, p. 335. DOI: 10.1007/BF00155184.

Cheng X., Zhang J., Saar S.H., Ding M.D. Differential emission measure analysis of multiple structural components of coronal mass ejections in the inner corona. *Astrophys. J.* 2012, vol. 761, no. 1, 62. DOI: 10.1088/0004-637X/761/1/62.

Chiuderi Drago F., Alissandrakis C., Hagyard M. Microwave emission above steady and moving sunspots. *Solar Phys.* 1987, vol. 112, p. 89. DOI: 10.1007/BF00148490.

Christe S., Hannah I.G., Krucker S., McTiernan J., Lin R.P. RHESSI microflare statistics. I. Flare-finding and frequency distributions. *Astrophys. J.* 2008, vol. 677, p. 1385. DOI: 10.1086/529011.

Fleishman G.D. Generation of resonance transition emissions in the solar atmosphere. *Astronomy Lett*. 2001, vol. 27, p. 254. DOI: 10.1134/1.1358383.

Fleishman G.D., Mel'nikov V.F. Reviews of topical problems: Millisecond solar radio spikes. *Physics-Uspekhi* [Adv. Phys. Sci.]. 1998, vol. 41, iss. 12, pp. 1157–1189. DOI: 10.1070/ PU1998v041n12ABEH000510.

Fleishman G.D., Nita G.M., Gary D.E. Evidence for Resonant Transition Radiation in Decimetric Continuum Solar Bursts. *Astrophys. J.* 2005, vol. 620, p. 506. DOI: 10.1086/427022.

Gary D.E., Hartl M.D., Shimizu T. Nonthermal radio emission from solar soft X-ray transient brightenings. *Astrophys. J.* 1997, vol. 477, p. 958. DOI: 10.1086/303748.

Ginzburg V.L., Syrovatskii S.I. Cosmic Magnetobremsstrahlung (synchrotron Radiation). *Ann. Rev. Astron. Astrophys.* 1965, vol. 3, p. 297. DOI: 10.1146/annurev.aa.03.090165.001501.

Gopalswamy N., Zhang J., Kundu M.R., Schmahl E.J., Lemen J.R. Fast time structure during transient microwave brightenings: Evidence for nonthermal processes. *Astrophys. J.* 1997, vol. 491, pp. L115–L119. DOI: 10.1086/311063.

Gudiksen B.V., Nordlund A. An ab initio approach to solar coronal loops. *Astrophys. J.* 2005, vol. 618, no. 2, p. 1031. DOI: 10.1086/426064.

Hannah I.G., Christe S., Krucker S., Hurford G.J., Hudson H.S., Lin R.P. RHESSI microflare statistics. II. X-ray imaging, spectroscopy, and energy distributions. *Astrophys. J.* 2008, vol. 677, p. 704. DOI: 10.1086/529012.

Hannah I.G., Hudson H.S., Battaglia M., Christe S., Kašparová J., Krucker S., Kundu M.R., Veronig A. Microflares and the statistics of X-ray flares. *Space Sci. Rev.* 2011, vol. 159, 263. DOI: 10.1007/s11214-010-9705-4.

Klimchuk J.A. On solving the coronal heating problem. *Solar Phys.* 2006, vol. 234, iss. 1, p. 41. DOI: 10.1007/s11207-006-0055-z.

Kosugi T., Matsuzaki K., Sakao T., Shimizu T., Sone Y., Tachikawa S., Hashimoto T., Minesugi K., Ohnishi A., et al. The Hinode (Solar-B) Mission: An overview. *Solar Phys.* 2007, vol. 243, p. 3. DOI: 10.1007/s11207-007-9014-6.

Kundu M.R., Schmahl E.J., Grigis P.C., Garaimov V.I., Shibasaki K. Nobeyama radio heliograph observations of RHESSI microflares. *Astron. Astrophys.* 2006, vol. 451, iss. 2, p. 691. DOI: 10.1051/0004-6361:20053987.

Lemen J.R., Title A.M., Akin D.J., Boerner P.F., Chou C., Drake J.F., Duncan D.W., Edwards C.G., et al. The Atmospheric Imaging Assembly (AIA) on the Solar Dynamics Observatory (SDO). *Solar Phys.* 2012, vol. 275, p. 17. DOI: 10.1007/s11207-011-9776-8.

Lesovoi S.V., Altyntsev A.T., Ivanov E.F., Gubin A.V. A 96-antenna radioheliograph. *Res. Astron. Astrophys.* 2014, vol. 14, iss. 7, pp. 864–868. DOI: 10.1088/1674-4527/14/7/008.

Lesovoi S., Altyntsev A., Kochanov A., Grechnev V.V., Gubin A.V., Zhdanov D.A., Ivanov E.F., et al. Siberian Radioheliograph: first results. *Solar-Terr. Phys.* 2017, vol. 3, iss. 1, p. 3. DOI: 10.12737/article_58f96ec60fec52.86165286.

Li Y., Fleishman G. Radio emission from acceleration sites of solar flares. *Astrophys. J.* 2009, vol. 701, p. L52. DOI: 10.1088/0004-637X/701/1/L52.

Lin R.P., Schwartz R.A., Kane S.R., Pelling R.M., Hurley K.C. Solar hard X-ray microflares. *Astrophys. J.* 1984, vol. 283, p. 421. DOI: 10.1086/162321.

Lopez Fuentes M.C., Klimchuk J.A. A simple model for

the evolution of multi-stranded coronal loops. *Astrophys. J.* 2010, vol. 719, p. 591. DOI: 10.1088/0004-637X/719/1/591.

Mandrini C.H., Démoulin P., Klimchuk J.A. Magnetic field and plasma scaling laws: Their implications for coronal heating models. *Astrophys. J.* 2000, vol. 530, p. 999. DOI: 10.1086/308398.

Meegan C., Lichti G., Bhat P.N., Bissaldi E., Briggs M.S., Connaughton V., Diehl R., Fishman G., et al. The Fermi Gamma-ray Burst Monitor. *Astrophys. J.* 2009, vol. 702, p. 791. DOI: 10.1088/0004-637X/702/1/791.

Meshalkina N.S., Altyntsev A.T., Zhdanov D.A., Lesovoi S.V., Kochanov A.A., Yan Y.H., Tan C.M. Study of flare energy release using events with numerous type III-like bursts in microwaves. *Solar Phys.* 2012, vol. 280, p. 537. DOI: 10.1007/s11207-012-0065-y.

Myachin D.Y., Nefedyev V.P., Uralov A.M., Lesovoi S.V., Smolkov G.Ya. Evolution of active regions in microwave emission at the stage of their initiation. *Proc. Nobeyama Symp*. 1999, vol. 479, p. 89.

Nakajima H., Nishio M., Enome S., Shibasaki K., Takano T., Hanaoka Y., Torii C., Sekiguchi H., Bushimata T., et al. The Nobeyama radioheliograph. *IEEE Proc.* 1994, vol. 82, p. 705.

Nefed'ev V.P., Agalakov B.V., Kardapolova N.N., Smol'kov G.Ya. The detection of the S-component sunspot source in the initial stage of active-region development. *Ann. Geophys.* 1993, vol. 11, no. 7, p. 614.

Nindos A., Kundu M.R., White S.M. A study of microwave selected coronal transient brightenings. *Astrophys. J.* 1999, vol. 513, p. 983. DOI: 10.1086/306886.

Panesar N.K., Sterling A.C., Moore R.L. Magnetic flux cancellation as the origin of solar quiet-region pre-jet minifilaments. *Astrophys. J.* 2017, vol. 844, 131. DOI: 10.3847/1538-4357/aa7b77.

Panesar N.K., Sterling A.C., Moore R.L Magnetic flux cancelation as the trigger of solar coronal jets in coronal holes. *Astrophys. J.* 2018, vol. 853, 189. DOI: 10.3847/1538-4357/aaa3e9.

Parker E.N. Nanoflares and the solar X-ray corona. *Astrophys. J.* 1988, vol. 330, p. 474. DOI: 10.1086/166485.

Pesnell W.D., Thompson B.J., Chamberlin P.C. The Solar Dynamics Observatory (SDO). *Solar Phys.* 2012, vol. 275, p. 3. DOI: 10.1007/s11207-011-9841-3.

Porter J.G., Toomre J., Gebbie K.B. Frequent ultraviolet brightenings observed in a solar active region with solar maximum mission. *Astrophys. J.* 1984, vol. 283, p. 879. DOI: 10.1086/162375.

Rudenko G.V., Anfinogentov S.A. Very fast and accurate azimuth disambiguation of vector magnetograms. Solar Phys. 2014, vol. 289, p. 1499. DOI: 10.1007/s11207-013-0437-y.

Schadee A., de Jager C., Svestka Z. Enhanced X-ray emission above 3.5-KEV in active regions in the absence of flares. *Solar Phys.* 1983, vol. 89, p. 287. DOI: 10.1007/BF00217252.

Scherrer P.H., Schou J., Bush R.I., Kosovichev A.G., Bogart R.S.,·Hoeksema J.T., Liu Y., et al. The Helioseismic and Magnetic Imager (HMI) investigation for the Solar Dynamics Observatory (SDO). *Solar Phys.* 2012, vol. 275, p. 207. DOI: 10.1007/s11207-011-9834-2.

Schou J., Scherrer P.H., Bush R.I., Wachter R., Couvidat S., Rabello-Soares M.C., Bogart R.S., Hoeksema J.T., et al. Design and ground calibration of the Helioseismic and Magnetic Imager (HMI) Instrument on the Solar Dynamics Observatory (SDO). *Solar Phys.* 2012, vol. 275, p. 229. DOI: 10.1007/s11207-011-9842-2.

Shibasaki K., Chiuderi-Drago F., Melozzi M., Slottje C., Antonucci E. Microwave, ultraviolet, and soft X-ray observations of hale region 16898. *Solar Phys.* 1983, vol. 89, p. 307. DOI: 10.1007/BF00217253.

Shibata K., Nozawa S., Matsumoto R. Magnetic reconnection associated with emerging magnetic flux. *Publ. Astron. Soc. Japan.* 1992, vol. 44, p. 265.

Shimizu T., Tsuneta S., Acton L.W., Lemen J.R., Ogawara Y., Uchida Y. Morphology of active region transient brightenings with the YOHKOH Soft X-Ray Telescope. *Astrophys. J.* 1994, vol. 422, p. 906. DOI: 10.1086/173782.

Thomas R., Starr R., Crannell C. Expressions to determine temperatures and emission measures for solar X-ray events from GOES measurements. *Solar Phys*. 1985, vol. 95, p. 323. DOI: 10.1007/BF00152409.

Trubnikov B.A. Particle interactions in a fully ionized plasma. *Rev. Plasma Phys*. 1965, vol. 1, p. 105.

Warnecke J., Peter H. Data-driven model of the solar corona above an active region. *Astron. Astrophys*. 2019, vol. 624, id. L12, p. 5. DOI: 10.1051/0004-6361/201935385.

White S.M., Kundu M.R., Shimizu T., Shibasaki K., Enome S. The radio properties of solar active region soft X-ray transient brightenings. *Astrophys. J.* 1995, vol. 450, p. 435. DOI: 10.1086/176153.

Wright P.J., Hannah I., Grefenstette B., Glesener L., Krucker S., Hudson H.S., et al. Microflare heating of an active region observed with NuSTAR, Hinode/XRT, and SDO/AIA. *Astrophys. J.* 2017, vol. 844, 132. DOI: 10.3847/1538-4357/aa7a59.

Yasnov L.V., Bogod V.M., Fu Q., Yan Y. A study of non-thermal radio emission features using fine spectral BAO and high-sensitivity RATAN observations of a solar active region. *Solar Phys.* 2003, vol. 215, p. 343. DOI: 10.1023/A:1025666810398.

Yokoyama T., Shibata K. Magnetic reconnection as the origin of X-ray jets and Hα surges on the Sun. *Nature*. 1995, vol. 375, p. 42. DOI: 10.1038/375042a0.

Yokoyama T., Shibata K. Numerical simulation of solar coronal X-ray jets based on the magnetic reconnection model. *Publ. Astron. Soc. Japan*. 1996, vol. 48, pp. 353–376. DOI: 10.1093/pasj/48.2.353.

Young P.R., Tian H., Peter H., Rutten R.J.,·Nelson C.J., Huang Z., Schmieder B., Vissers G.J.M., Toriumi S., et al. Solar ultraviolet bursts. *Space Sci. Rev.* 2018, vol. 214, iss. 8, 120, 39 p. DOI: 10.1007/s11214-018-0551-0.

Zaitsev V.V., Stepanov A.V. The plasma radiation of flare kernels. *Solar Phys.* 1983, vol. 88, p. 297. DOI: 10.1007/BF00196194.

Zaitsev V.V., Kruger A., Hildebrandt J., Kliem B. Plasma radiation of power-law electrons in magnetic loops: Application to solar decimeter-wave continua. *Astron. Astrophys.* 1997, vol. 328, p. 390.

Zhang J., Kundu M.R., White S.M., Dere K.P., Newmark J.S. Reconciling extreme-ultraviolet and radio observations of the Sun's corona. *Astrophys. J.* 2001, vol. 561, p. 396. DOI: 10.1086/323212.

Zhdanov D.A., Zandanov V.G. Broadband microwave spectropolarimeter. *Central European Astrophysical Bulletin.* 2011, vol. 35, p. 223.

Original Russian version: A.T. Altyntsev, N.S. Meshalkina, I.I. Myshyakov, published in Solnechno-zemnaya fizika. 2022. Vol. 8. Iss. 2. P. 4–11. DOI: 10.12737/szf-82202201. © 2022 INFRA-M Academic Publishing House (Nauchno-Izdatelskii Tsentr INFRA-M)

How to cite this article

Altyntsev A.T., Meshalkina N.S., Myshyakov I.I. Coherent microwave emission as an indicator of non-thermal energy release at a coronal X-ray point. *Solar-Terrestrial Physics*. 2022. Vol. 8. Iss. 2. P. 3–9. DOI: 10.12737/stp-82202201.